NASA TECHNICAL NOTE

NASA TN D-4098

$c.1$

NASA TN D-4098

AERODYNAMIC CHARACTERISTICS OF A SPHERICALLY BLUNTED 25° CONE AT A MACH NUMBER OF 20

by Julius E. Harris

Langley Research Center

Langley Station, Hampton, Va.

AERODYNAMIC CHARACTERISTICS OF A SPHERICALLY

BLUNTED 25° CONE AT A MACH NUMBER OF 20

By Julius E. Harris

Langley Research Center
Langley Station, Hampton, Va.

NATIONAL AERONAUTICS AND SPACE ADMINISTRATION

AERODYNAMIC CHARACTERISTICS OF A SPHERICALLY
BLUNTED 25° CONE AT A MACH NUMBER OF 20

By Julius E. Harris
Langley Research Center

SUMMARY

An experimental investigation has been conducted in nitrogen to determine the static longitudinal aerodynamic characteristics and the pressure distributions for a spherically blunted cone with a 25° semiapex angle. The bluntness ratio of the configuration, defined as the ratio of nose radius to base radius, was 0.2. The tests were made in the Langley hotshot tunnel at a Mach number of approximately 20 and a Reynolds number, based on cone base diameter, of 0.15×10^6. Static longitudinal-stability data and pressure-distribution data were obtained over angle-of-attack ranges of 0° to 30° and 0° to 15°, respectively.

Analysis of the data indicated that the configuration was statically stable for a center of gravity at the centroid of the planform area. The maximum lift-drag ratio was approximately 0.563 and occurred at an angle of attack of 20°. The lift and drag coefficients corresponding to the maximum lift-drag ratio were 0.369 and 0.655, respectively. The maximum lift coefficient was 0.395 and occurred at an angle of attack of 25°. The slopes evaluated at zero angle of attack of the curves for lift coefficient and pitching-moment coefficient as functions of angle of attack were 0.023 deg^{-1} and -0.0054 deg^{-1}, respectively.

Estimates of the force and moment coefficients obtained by using modified Newtonian impact theory agreed well with the trends of the experimental results over the angle-of-attack range and, in many instances, predicted the actual magnitudes within the accuracy of the experimental data. Pressure coefficients estimated by using modified Newtonian impact theory were in good agreement with those obtained on the spherical nose but were less than those obtained on the conical portion of the configuration. Predictions with tangent-cone theory of the conical pressure coefficients agreed well with the experimental data.

INTRODUCTION

Spherically blunted cones are among the configurations of interest for entry vehicles. These configurations are basic geometric shapes and have been the subject of both

analytical and experimental research for a number of years. During these studies considerable data have been accumulated for a rather broad range of Mach numbers, Reynolds numbers, cone angles, and bluntness ratios. However, a shortage of information still exists in some areas, particularly for cone angles greater than 10° and Mach numbers greater than 10. (See, for example, the extensive literature survey presented in ref. 1.) Because of this lack of information, an experimental program was conducted in the Langley hotshot tunnel to determine the static longitudinal stability characteristics and the pressure distributions for a spherically blunted cone having a 25° semiapex angle and a bluntness ratio of 0.2. The tests were made at a Mach number of approximately 20 and a Reynolds number, based on cone base diameter, of 0.15×10^6.

SYMBOLS

C_A axial-force coefficient

C_D drag coefficient, $C_N \sin \alpha + C_A \cos \alpha$

C_L lift coefficient, $C_N \cos \alpha - C_A \sin \alpha$

C_m pitching-moment coefficient

C_N normal-force coefficient

C_p pressure coefficient, $\dfrac{p - p_\infty}{q_\infty}$

d   cone base diameter

L/D lift-drag ratio, C_L / C_D

l length of model (see fig. 2)

M   Mach number

p   pressure

q   dynamic pressure, $\rho V^2 / 2$

$R_{\infty,d}$ Reynolds number, $\dfrac{\rho_\infty V_\infty d}{\mu_\infty}$

s   surface coordinate ($s \equiv 0$ at $x = y = 0$) (see fig. 2)

T   temperature

V   velocity

x,y   body coordinate system (see fig. 2)

x_{cp} center of pressure

α angle of attack

β meridian coordinate ($\beta = 0$ on most windward ray of cone and π on most leeward ray)

γ ratio of specific heats

μ coefficient of viscosity

ρ density

ϕ cone semiapex angle

Subscripts:

b   base of cone

max   maximum

t   total condition

∞ free stream

APPARATUS AND TESTS

Test Facility

The present investigation was conducted in the Langley hotshot tunnel. A detailed discussion on the operation and calibration of this facility is presented in reference 2.

The total pressure in the arc chamber was measured with strain-gage pressure transducers and recorded as a function of time during each test. This pressure, together with the initial arc-chamber density prior to arc discharge, was used to calculate the total temperature. Pitot pressure in the test section was measured as a function of time with a variable-reluctance transducer. This pressure, together with the arc-chamber total pressure and temperature as functions of time, was used to calculate the free-stream thermodynamic properties.

Models

The configuration used in the present investigation was a spherically blunted cone having a 25° semiapex angle and a bluntness ratio of 0.2. Bluntness ratio is defined herein as the ratio of the spherical-nose radius to the cone base radius. Sectional views of the models used for the force tests and pressure tests are presented in figure 1.

The model used for the force tests (fig. 1(a)) was integrally machined from a block of magnesium to minimize weight and, thus, to maximize balance response and weighed approximately 0.09 pound (40.8 g). The typical wall thickness was 0.03 inch (0.076 cm). A thin-wall (0.01 inch (0.025 cm) thick) stainless-steel cylinder was inserted into the balance can in order to insure a lasting fit between the model and balance. A 0.038-inch-diameter (0.096 cm) pressure orifice was located at the point $x = y = 0$.

The model used for the pressure tests (fig. 1(b)) was machined from AISI type 347 stainless steel in halves to allow access to the 10 internally mounted variable-reluctance pressure transducers. The orifice diameters were 0.038 inch (0.096 cm).

Instrumentation

A three-component, internally mounted strain-gage balance was used to measure the aerodynamic forces and moments exerted on the model during the investigation. The strain-gage outputs were amplified by a 3-kilocycle carrier amplifier and recorded on an oscillograph. The local pressure at the point $x = y = 0$ was measured with an internally mounted variable-reluctance pressure transducer over the range $0^{\circ} \leq \alpha \leq 30^{\circ}$. This pressure was corrected to the stagnation-point value by using a Newtonian correction and compared with the value obtained from the pitot tube. In general, these comparisons agreed to within ±3 percent and insured the correct dynamic pressure for the reduction of the force and moment data to coefficient form.

Local pressures on the model were measured with internally mounted variable-reluctance pressure transducers at 10 orifice locations. The outputs from these transducers were amplified by 20-kilocycle amplifiers and recorded on an oscillograph. The maximum length of tubing used to connect the transducers to the orifices was 1.5 inches

(3.81 cm). The reference side of the transducers was connected to a reference manifold which was evacuated to approximately 3 microns of mercury.

Test Conditions and Data Accuracy

The approximate test conditions for the present investigation are as follows:

M_∞ 20

$R_{\infty,d}$ . . . . 0.15 × 10^6

$p_{t,\infty}$, psia (MN/m^2) 11 000 (75.8)

$T_{t,\infty}$, $^\circ$R ($^\circ$K) 5400 (3000)

p_∞, psia (N/m^2) 0.002 (13.79)

T_∞, $^\circ$R ($^\circ$K) 86 (48)

Force tests α, deg . . . . 0 to 30

Pressure tests α, deg . . . . 0 to 15

Test gas . . . . Nitrogen ($\gamma = 1.4$)

The maximum anticipated uncertainties in the force, moment, and pressure coefficients resulting from any error in the strain-gage-balance measurements, the variable-reluctance-pressure-transducer measurements, and the carrier amplifier outputs are

C_N . . . . ±0.01

C_A . . . . ±0.01

C_m . . . . ±0.001

C_p . . . . ±0.01

THEORY

Estimates of the force and moment coefficients obtained by using modified Newtonian impact theory are compared with the experimental results. The equations presented in reference 3 for spherically blunted cones together with the tables presented in reference 4 were used to calculate the force and moment coefficients as functions of angle of attack. The tables presented in reference 4 are based on a stagnation pressure coefficient $C_{p,max}$ of 2.0; however, for the present investigation these tables were modified by assuming that

$$C_{p,max} = \frac{\gamma + 3}{\gamma + 1}\left[1 - \frac{2}{M_\infty{}^2(\gamma + 3)}\right] \qquad (1)$$

(See ref. 5.)

The pressure coefficients were predicted by using both Newtonian impact theory modified by equation (1) and tangent-cone theory. The modified Newtonian impact theory expression for the pressure coefficient is

$$C_p = C_{p,max}(\cos \alpha \sin \phi + \sin \alpha \cos \phi \cos \beta)^2 \tag{2}$$

For the cone rays of interest in the present investigation, equation (2) becomes for $\beta = 0$

$$C_p = C_{p,max} \sin^2(\alpha + \phi) \tag{3}$$

and for $\beta = \pm \frac{\pi}{2}$

$$C_p = C_{p,max} \cos^2\alpha \sin^2\phi \tag{4}$$

The relation

$$C_p = C_{p,max} \cos^2\theta \tag{5}$$

was used to calculate the pressure coefficients on the spherical nose for $\beta = 0$ and $\beta = \pm \frac{\pi}{2}$ over the angle-of-attack range. In equation (5) θ is the angle between the free-stream velocity direction and the normal to the surface. Tangent-cone theory was also used to predict the pressure coefficients on the conical portion of the configuration. In this instance the charts presented in reference 6 were used for an equivalent cone angle defined as $\alpha + \phi$.

RESULTS AND DISCUSSION

The sign convention for the force and moment coefficients, the coordinate system, and the moment reference center for this investigation are presented in figure 2.

The static longitudinal aerodynamic characteristics are presented in figure 3. The reference area and reference length for the coefficients are $\pi d^2/4$ and d, respectively. The normal-force coefficient C_N was nearly a linear function of angle of attack for $\alpha \leq 15°$. This linear trend of C_N as a function of α is in agreement with the results presented in figure 4 of reference 1 for a wide range of Mach numbers, cone angles, and bluntness ratios. The slope of C_N as a function of α evaluated at zero angle of attack was 0.0295 deg^{-1} as compared with the modified Newtonian value of 0.0274 deg^{-1}. (See fig. 3(a).) Modified Newtonian impact theory predicted the trend of C_N as a function of α, but underestimated the magnitude of C_N at $\alpha = 30°$ by approximately 10 percent. The trend of C_A as a function of α was also predicted, but as with C_N the values of C_A were less than the experimental results.

The slope evaluated at the trim point ($\alpha = 0°$) of C_m as a function of α was approximately -0.0054 deg^{-1} as compared with a modified Newtonian value of -0.0044 deg^{-1}. (See fig. 3(b).) The agreement between modified Newtonian impact theory estimates of the center of pressure and the experimental results improved with increasing angle of attack.

6

The lift and drag coefficients together with the lift-drag ratio are presented in figure 3(c). Modified Newtonian theory predicted the trend of C_D with angle of attack, but somewhat underpredicted the actual magnitudes. The slope evaluated at $\alpha = 0^O$ of the curve for C_L as a function of α was approximately 0.023 deg^{-1} as compared with the modified Newtonian value of 0.0215 deg^{-1}. Both the trend and magnitude of C_L were predicted over the angle-of-attack range. The maximum lift coefficient which occurred at $\alpha = 25^O$ was 0.395. The maximum lift-drag ratio was approximately 0.563 and occurred at $\alpha = 20^O$. Corresponding values of C_L and C_D for $(L/D)_{max}$ were 0.369 and 0.655, respectively.

The experimental pressure coefficients are presented in figure 4. It appears from the trend of the data that, with increasing s/s_b, an overexpansion occurred with the minimum pressure occurring in the interval $0.112 \leq \frac{s}{s_b} \leq 0.220$. Estimates of the pressure coefficients on the spherical nose obtained by using modified Newtonian impact theory (eq. (5)) agreed well with the experimental data for all values of α and β. However, with the exception of the data for zero angle of attack, modified Newtonian impact theory underpredicted the experimental values on the conical portion of the configuration. (See figs. 4(a) to 4(g).) Estimates of the pressure coefficients on the conical portion of the configuration obtained by using tangent-cone theory agreed within the experimental accuracy of the data in most instances. (See fig. 4.)

Schlieren photographs for angles of attack of 0°, 5°, 10°, 15°, and 20° are presented in figure 5. These photographs were taken during the pressure-distribution investigation. The outlines of the pitot tube and the previously mentioned pressure reference manifold as well as the tube which connected the manifold to the vacuum pump system can be seen at the base of the model.

CONCLUDING REMARKS

The results of an experimental investigation to determine the static longitudinal aerodynamic characteristics and the pressure distributions for a spherically blunted cone having a 25° semiapex angle and a bluntness ratio of 0.2 have been presented. The tests were made in the Langley hotshot tunnel at a Mach number of approximately 20 and a Reynolds number, based on the cone base diameter, of 0.15×10^6. The static longitudinal characteristics were obtained over an angle-of-attack range from 0° to 30°. The pressure-distribution data were obtained along the most windward cone ray and along the ray located $\pi/2$ from the most windward ray for angles of attack from 0° to 15°.

The configuration was statically stable for a center of gravity at the centroid of the planform area. The slope evaluated at zero angle of attack of the curve for pitching moment as a function of angle of attack was -0.0054 deg^{-1}. The maximum lift-drag ratio

was approximately 0.563 and occurred at an angle of attack of 20°. The lift and drag coefficients corresponding to the maximum lift-drag ratio were 0.369 and 0.655, respectively. The maximum lift coefficient was 0.395 and occurred at an angle of attack of 25°. The slope evaluated at zero angle of attack of the curve for lift coefficient as a function of angle of attack was 0.023 deg^{-1}.

Estimates of the force and moment coefficients obtained by using modified Newtonian impact theory agreed well with the trends of the experimental data and, in many instances, agreed with the actual magnitudes within the accuracy of the data. Pressure coefficients estimated by using modified Newtonian impact theory were in good agreement with those obtained on the spherical nose but were less than those obtained on the conical portion of the body. Predictions with tangent-cone theory agreed well with the results on the rearward portion of the conical body (downstream of the overexpansion).

Langley Research Center,
    National Aeronautics and Space Administration,
        Langley Station, Hampton, Va., March 1, 1967,
           124-07-02-54-23.

REFERENCES

1. Arnold, John W.; Simmons, Harmon L.; and Miller, William T.: An Investigation of the Aerodynamic Characteristics of a 25° Sphere-Cone Including a Pressure Distribution Analysis at Angles of Attack, and a Trajectory Analysis During a Typical Reentry Trajectory. Rept. No. NASA CR-66037, LTV Aerospace Corp., [1966].

2. Miller, Charles G., III; Creel, Theodore R., Jr.; and Smith, Fred M.: Calibration Experience in the Langley Hotshot Tunnel for Mach Numbers From 12 to 26. NASA TN D-3278, 1966.

3. Harris, Julius E.: Force-Coefficient and Moment-Coefficient Correlations and Air-Helium Simulation for Spherically Blunted Cones. NASA TN D-2184, 1964.

4. Wells, William R.; and Armstrong, William O.: Tables of Aerodynamic Coefficients Obtained From Developed Newtonian Expressions for Complete and Partial Conic and Spheric Bodies at Combined Angles of Attack and Sideslip With Some Comparisons With Hypersonic Experimental Data. NASA TR R-127, 1962.

5. Lees, Lester: Hypersonic Flow. Fifth Intern. Aeron. Conf. (Los Angeles, Calif.), Inst. Aeron. Sci., Inc., June 1955, pp. 241-276.

6. Ames Research Staff: Equations, Tables, and Charts for Compressible Flow. NACA Rept. 1135, 1953. (Supersedes NACA TN 1428.)
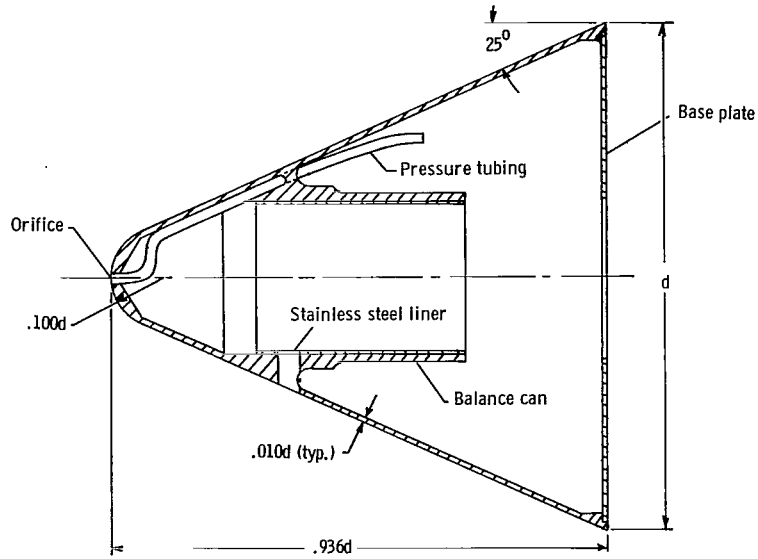
(a) Model used for force tests.

Orifice No.	x/d	s/s_b
1	0	0
2	.018	.056
3	.066	.112
4	.176	.220
5	.292	.338
6	.404	.455
7	.517	.569
8	.630	.686
9	.743	.800
10	.857	.926
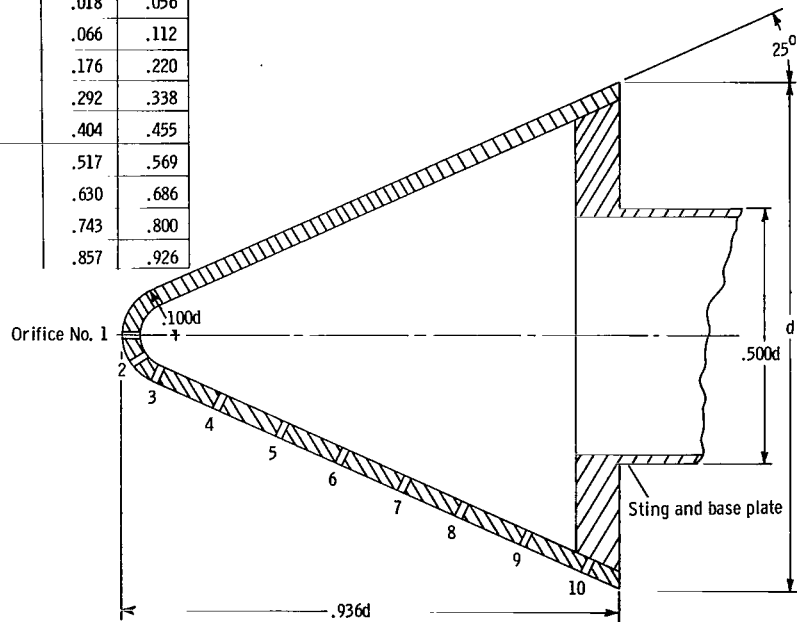
(b) Model used for pressure tests.

Figure 1.- Sectional view of models. d = 3.00 in. (7.62 cm).

Figure 2.- Sign convention. d = 3.00 in. (7.62 cm).
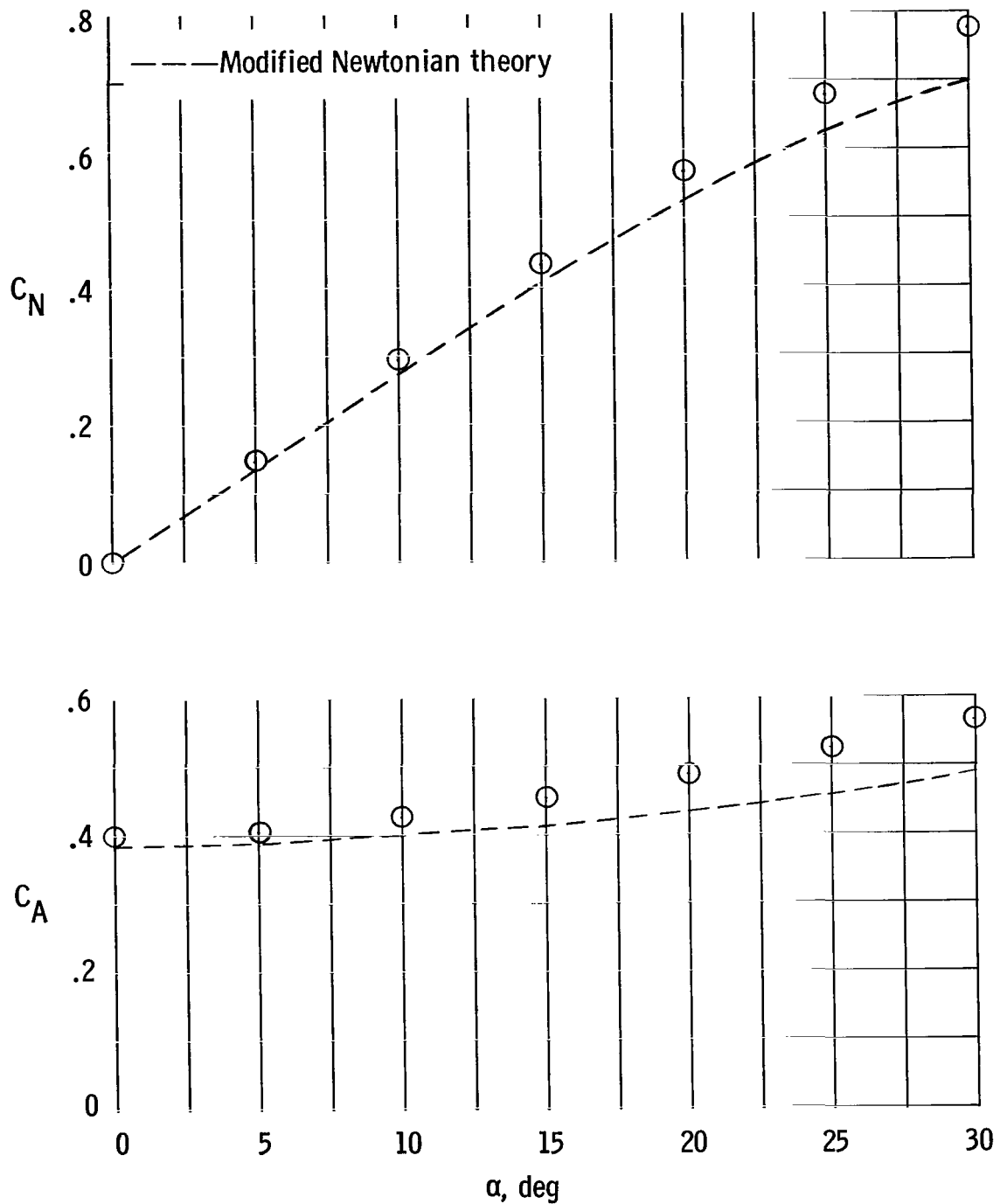
(a) C_N and C_A as a function of α.

Figure 3.- Static longitudinal aerodynamic characteristics. $M_\infty = 20$; $R_{\infty,d} = 0.15 \times 10^6$.
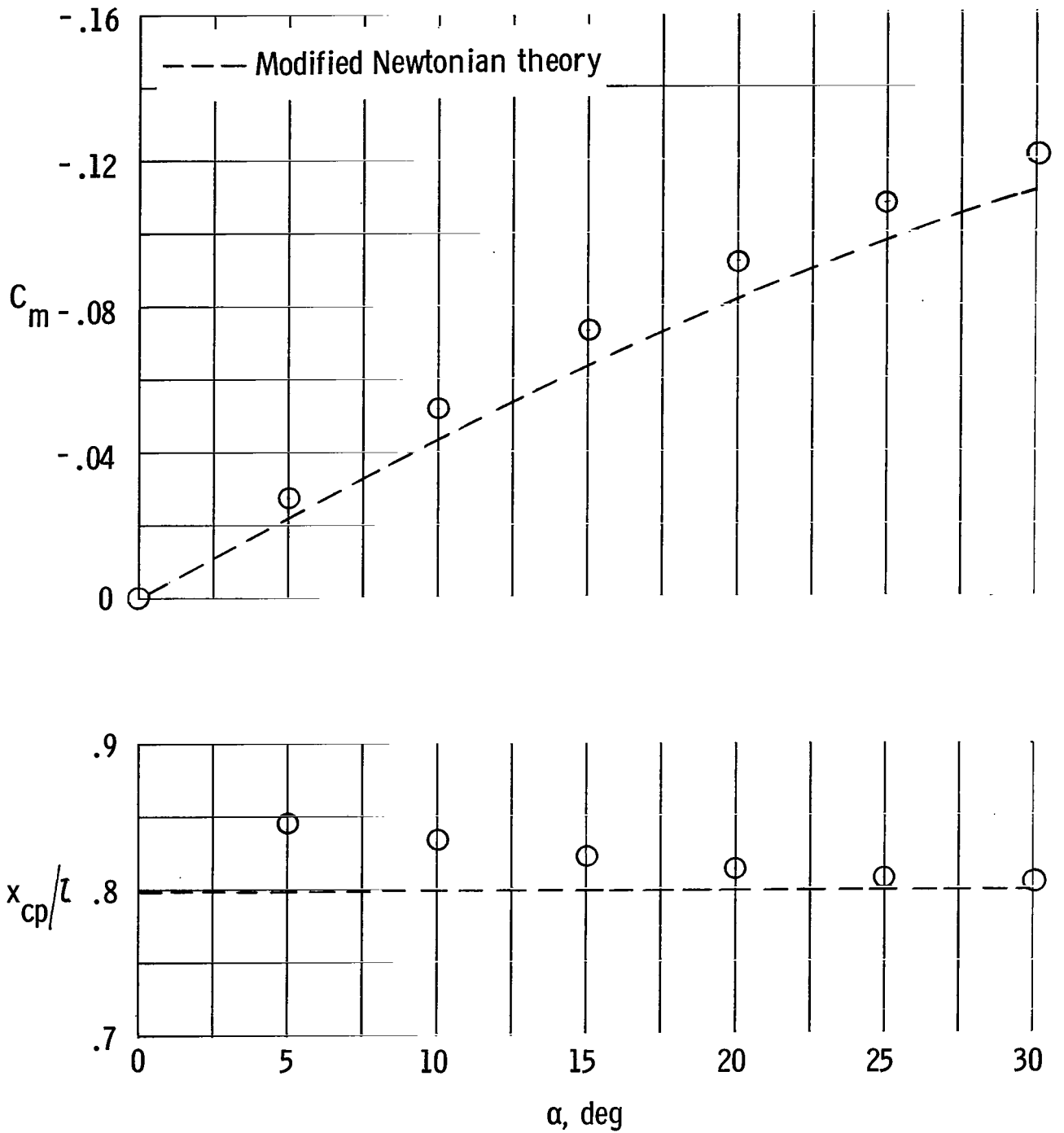
(b) C_m and x_{cp}/l as a function of α.

Figure 3.- Continued.
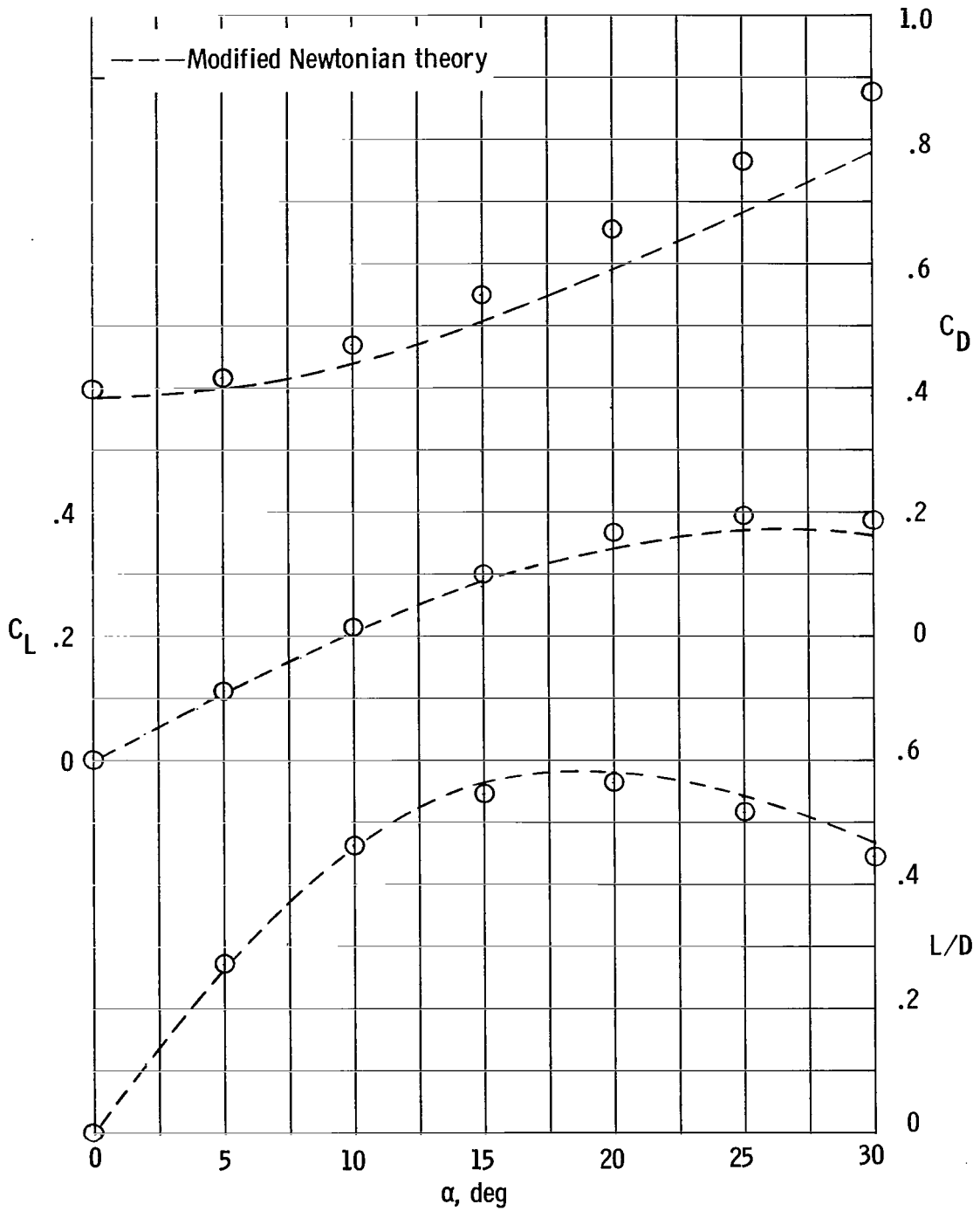
(c) C_L, C_D, and L/D as a function of α.

Figure 3.- Concluded.
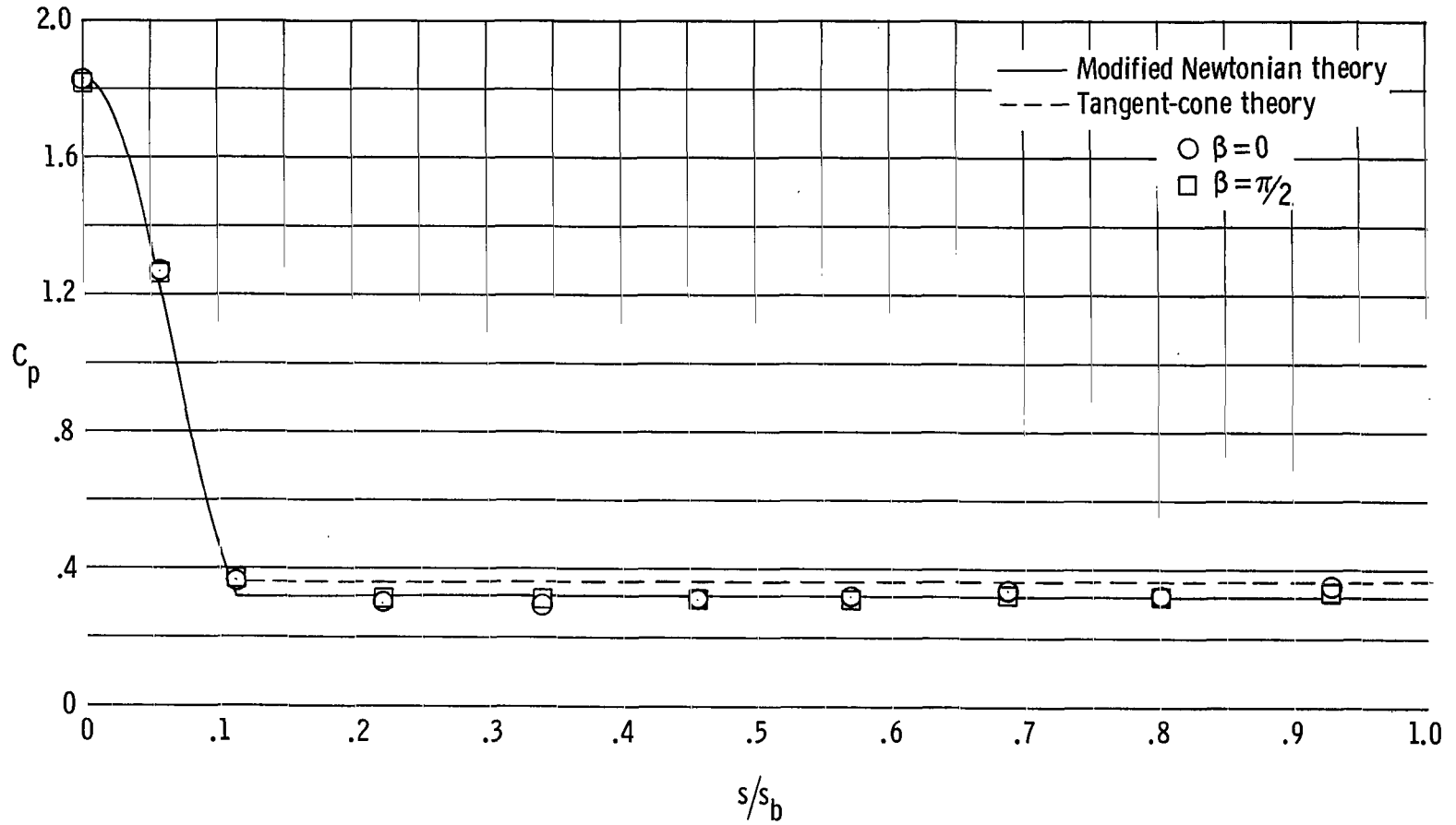
(a) $\alpha = 0^0$; $\beta = 0$ and $\pi/2$.

Figure 4.- Pressure-coefficient distribution. $M_\infty = 20$; $R_{\infty,d} = 0.15 \times 10^6$.

(b) $\alpha = 5^o$; $\beta = 0$.
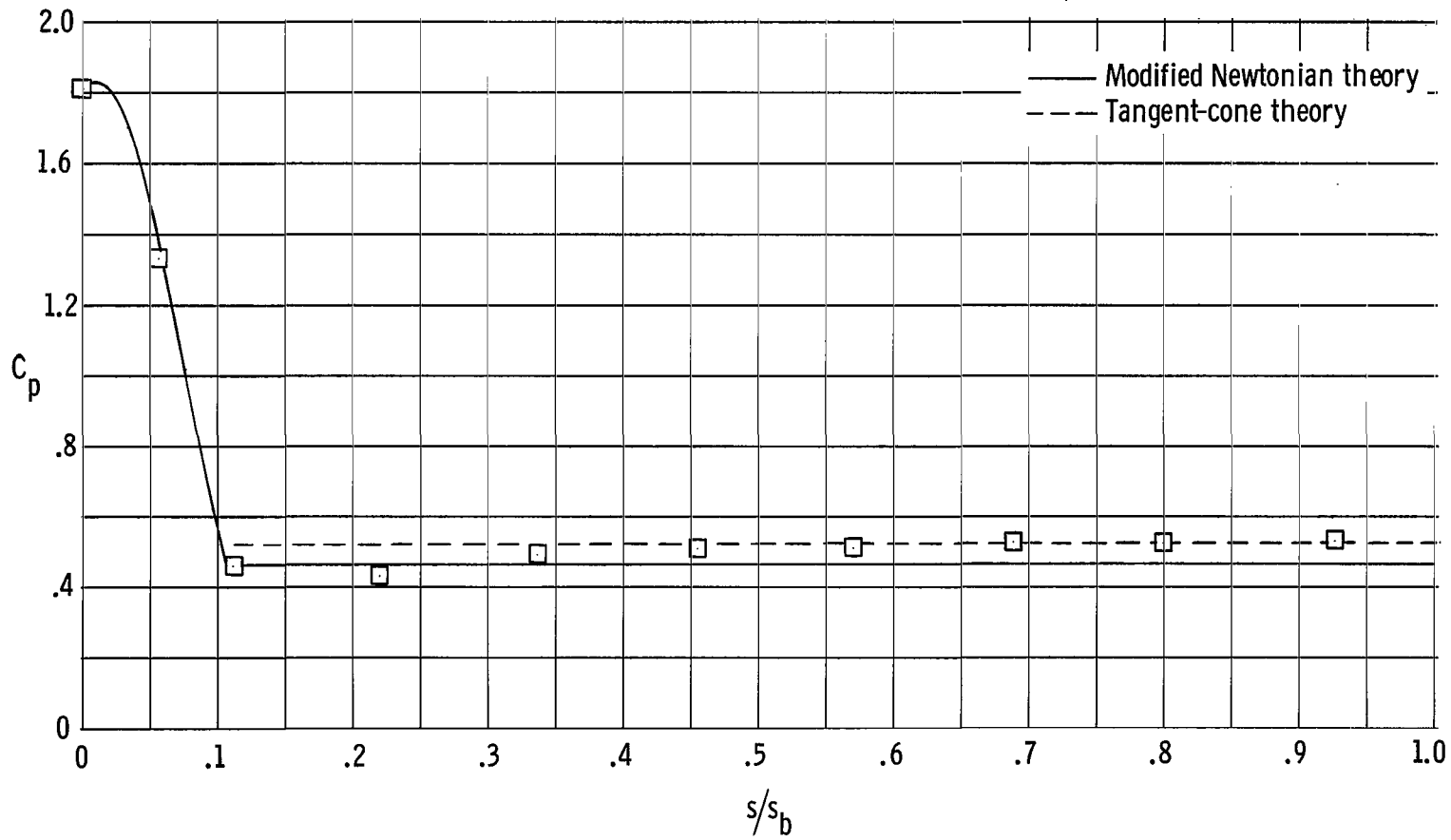
Figure 4.- Continued.

(c) $\alpha = 10^0$; $\beta = 0$.
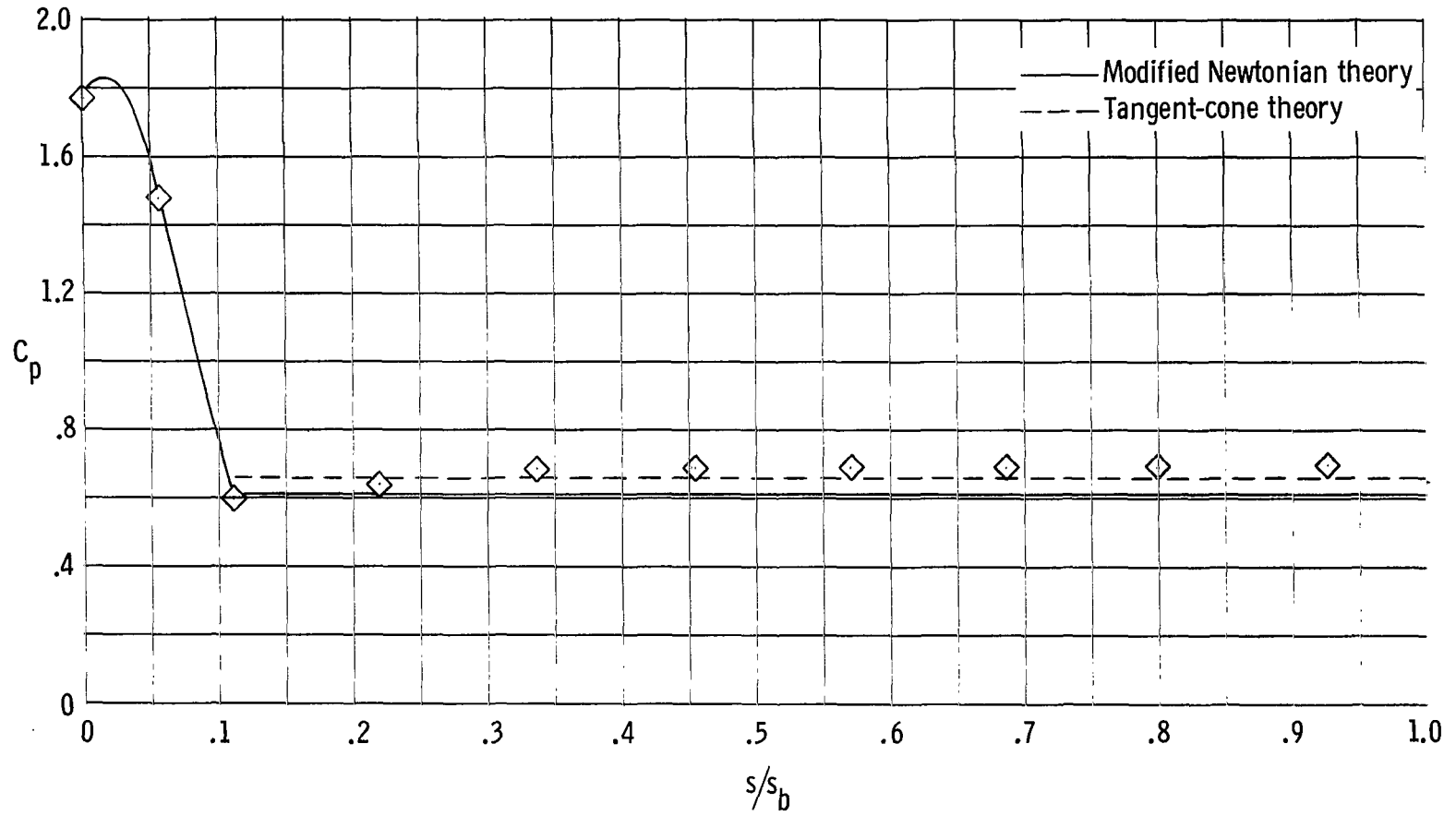
Figure 4.- Continued.

(d) $\alpha = 15^0$; $\beta = 0$.
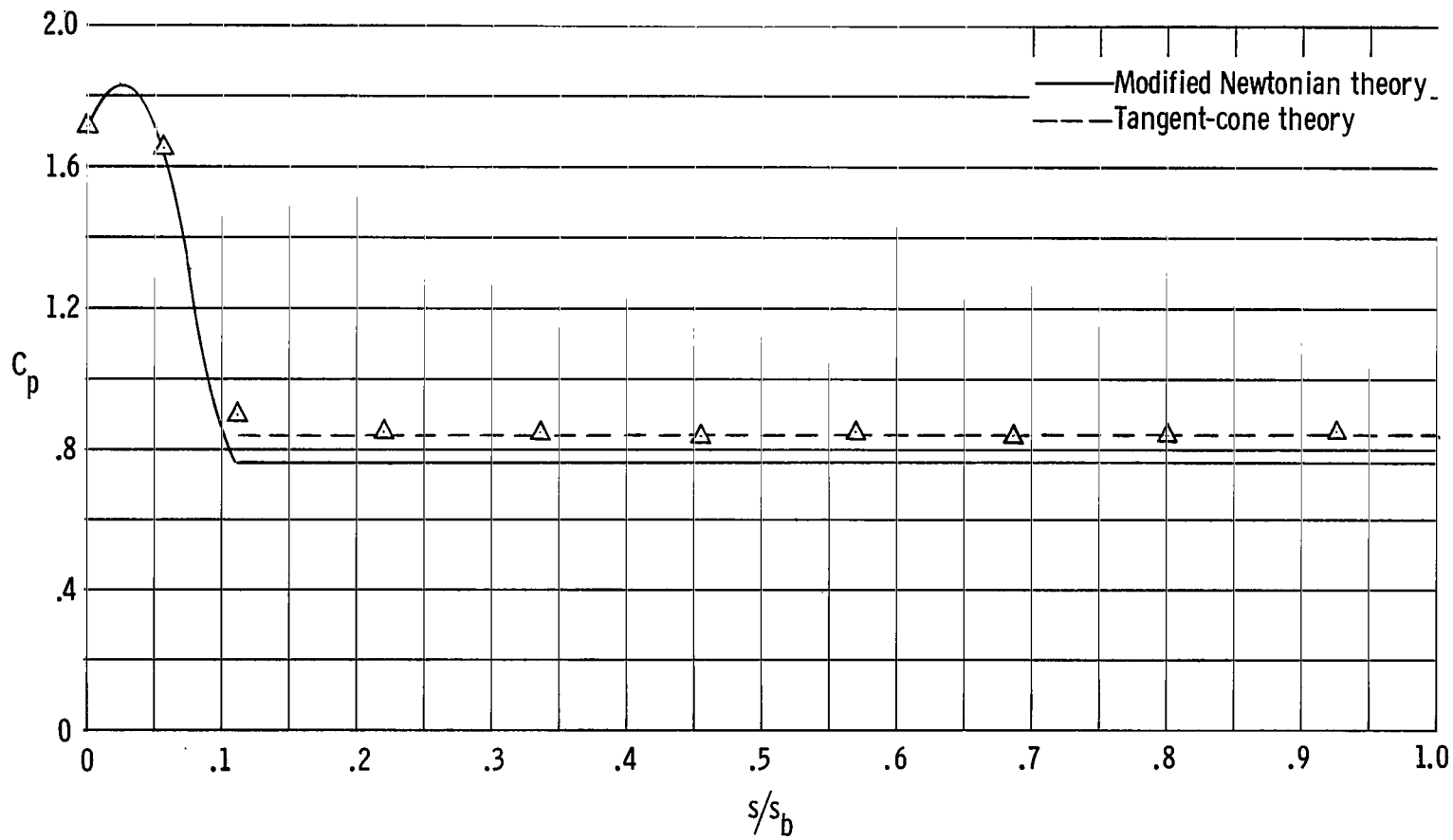
Figure 4.- Continued.

(e) $\alpha = 5^0$; $\beta = \pi/2$.
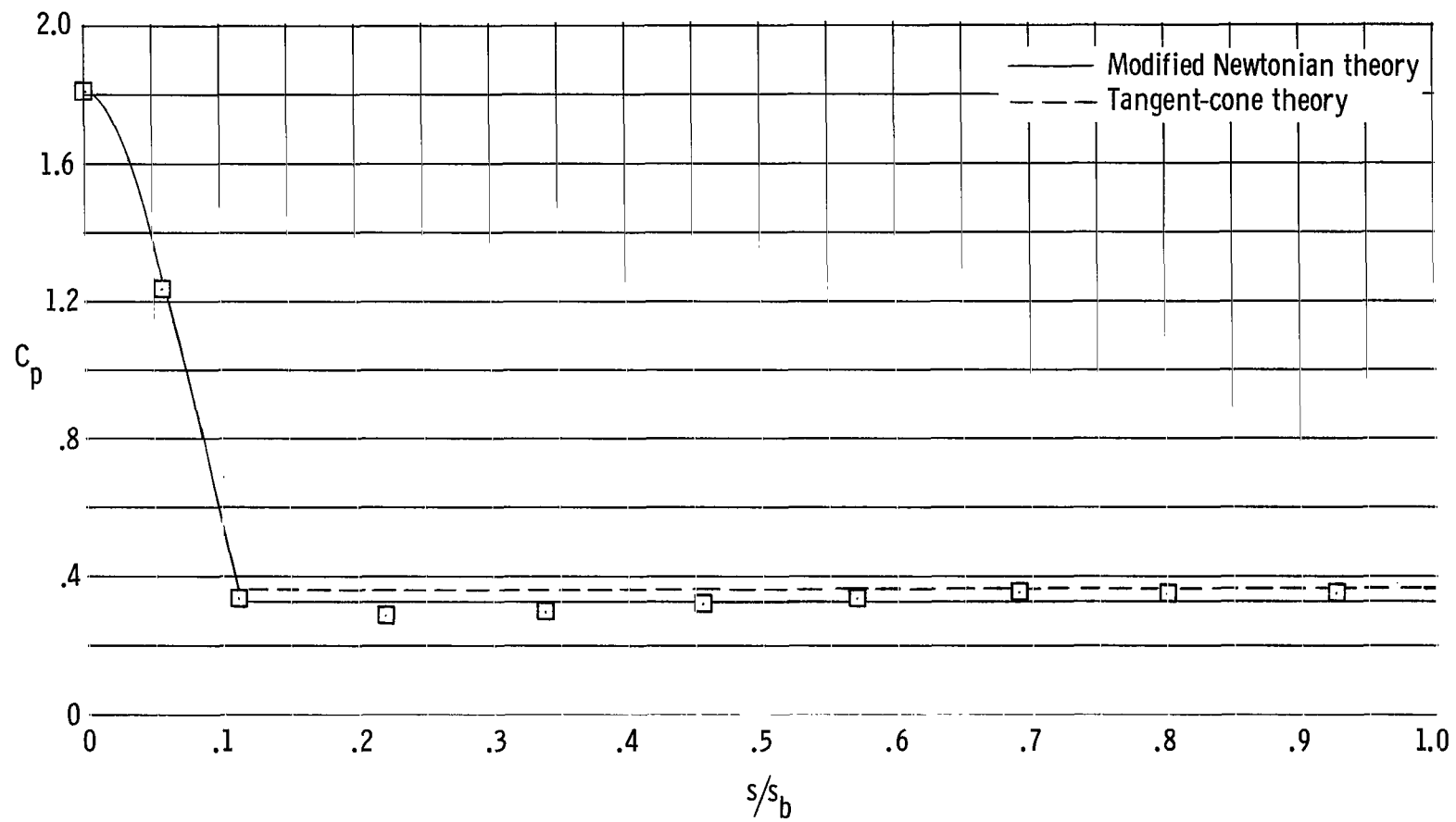
Figure 4.- Continued.

(f) $\alpha = 10^0$; $\beta = \pi/2$.
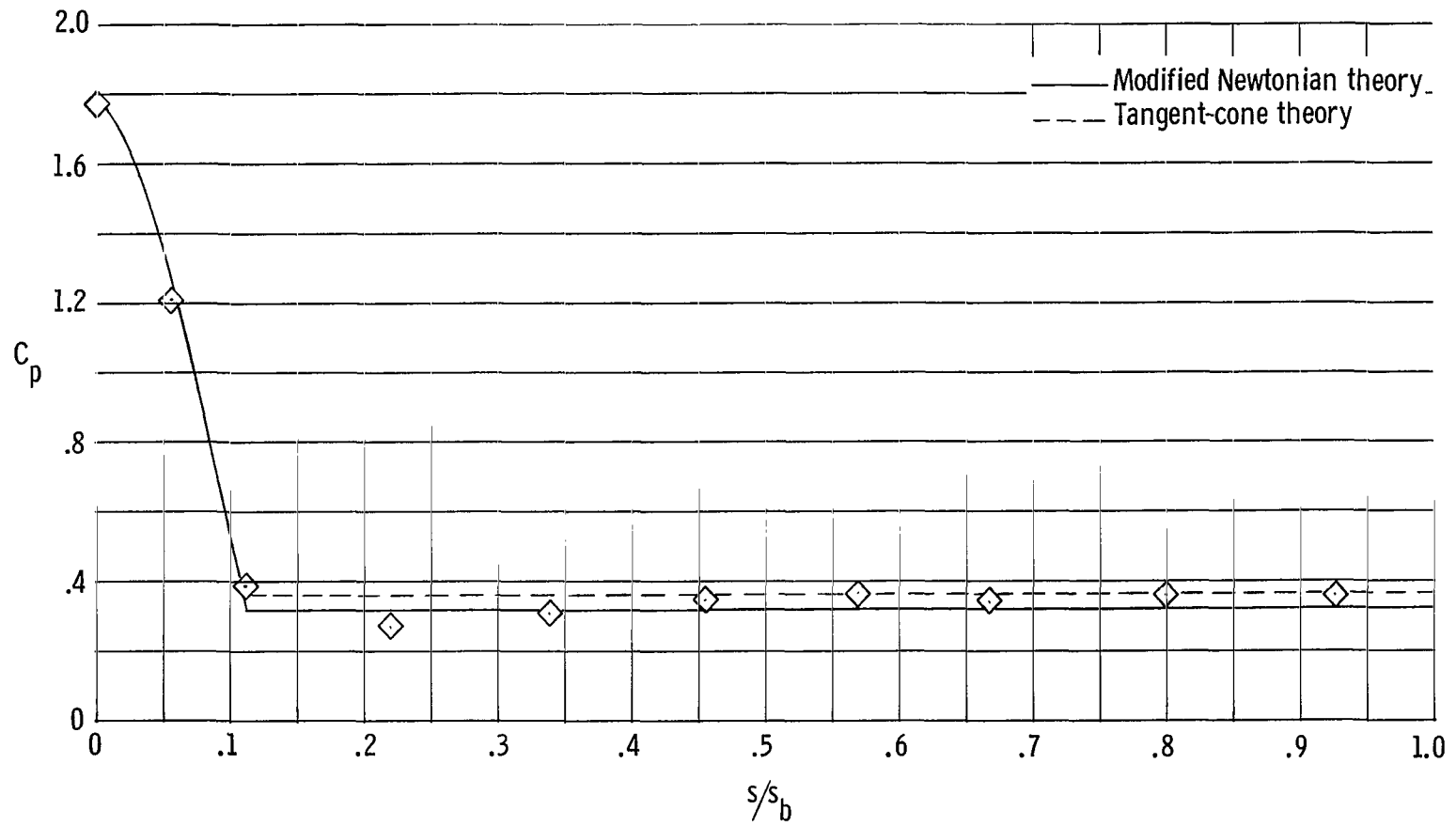
Figure 4.- Continued.
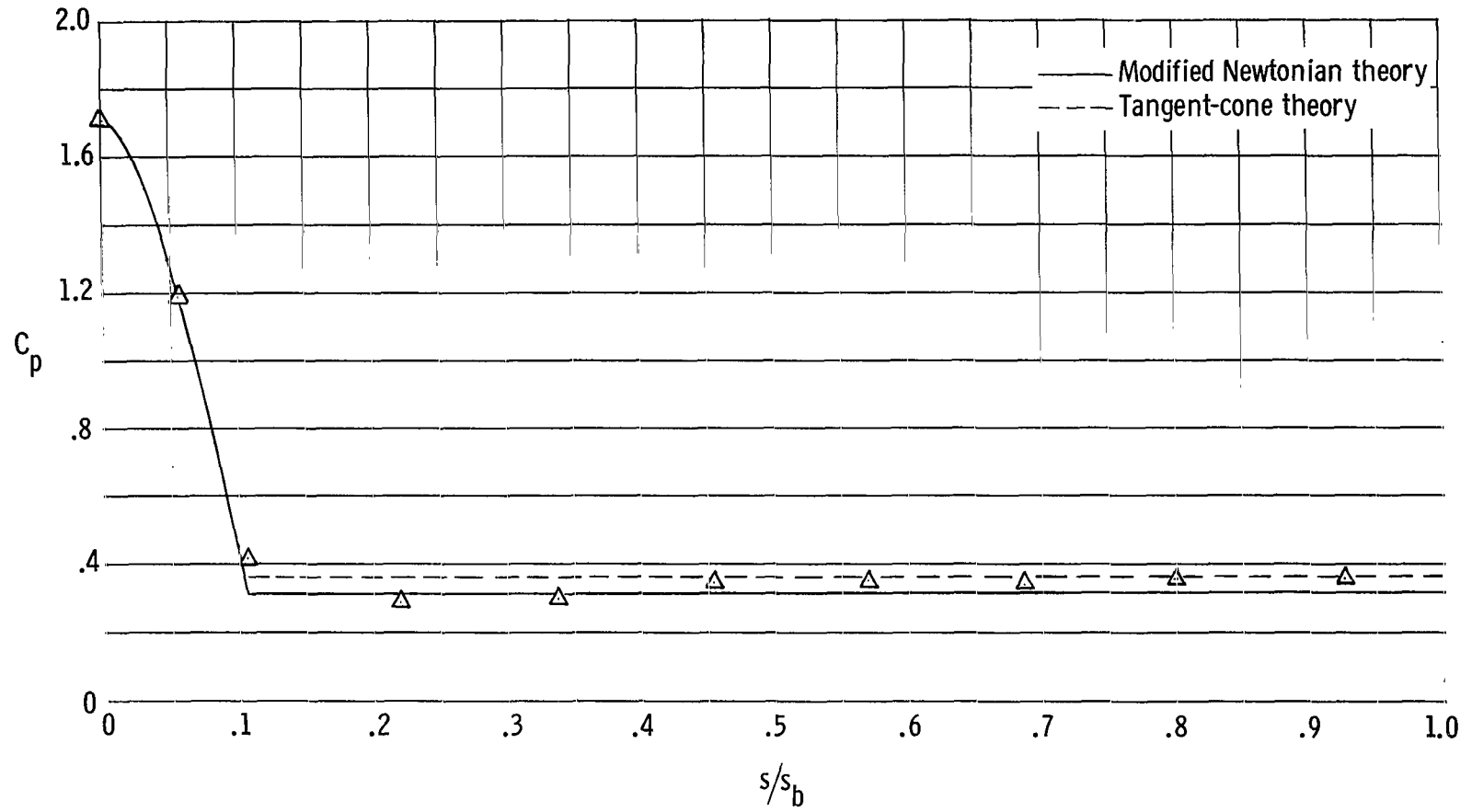
(g) $\alpha = 15^0$; $\beta = \pi/2$.

Figure 4.- Concluded.

$\alpha = 0^0$ $\alpha = 5^0$

$\alpha = 10^0$ $\alpha = 15^0$
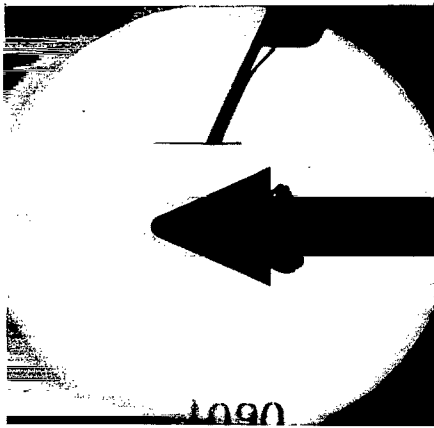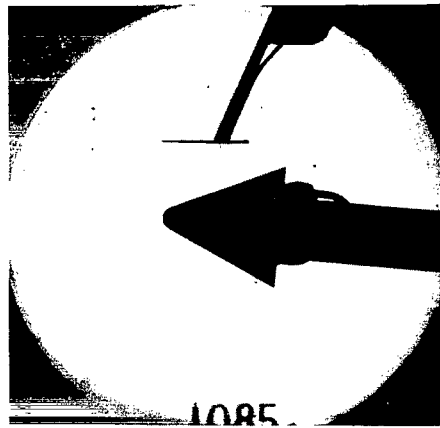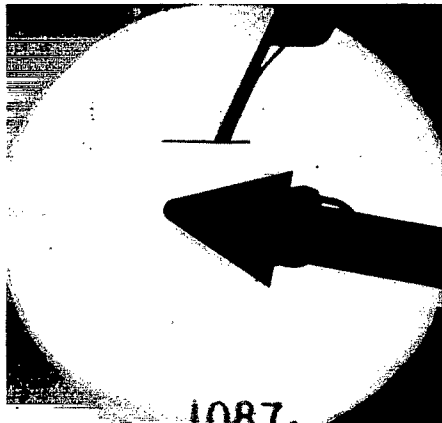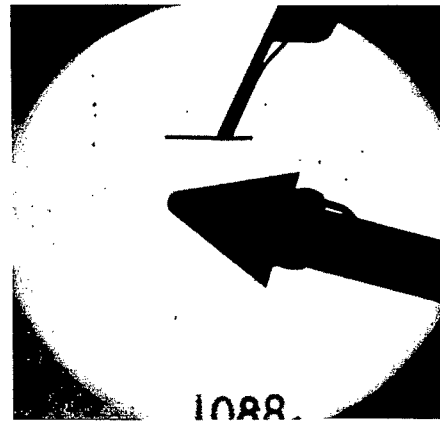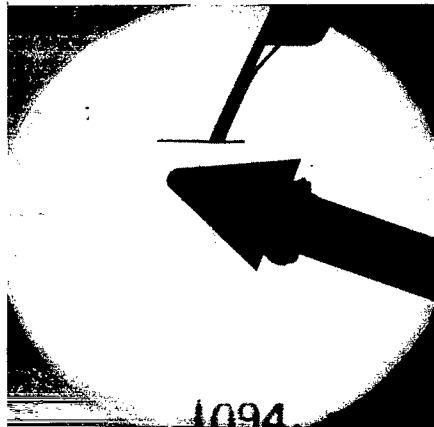
$\alpha = 20^0$

Figure 5.- Schlieren photographs.   L-67-972

NASA SCIENTIFIC AND TECHNICAL PUBLICATIONS

TECHNICAL REPORTS: Scientific and technical information considered important, complete, and a lasting contribution to existing knowledge.

TECHNICAL NOTES: Information less broad in scope but nevertheless of importance as a contribution to existing knowledge.

TECHNICAL MEMORANDUMS: Information receiving limited distribution because of preliminary data, security classification, or other reasons.

CONTRACTOR REPORTS: Scientific and technical information generated under a NASA contract or grant and considered an important contribution to existing knowledge.

TECHNICAL TRANSLATIONS: Information published in a foreign language considered to merit NASA distribution in English.

SPECIAL PUBLICATIONS: Information derived from or of value to NASA activities. Publications include conference proceedings, monographs, data compilations, handbooks, sourcebooks, and special bibliographies.

TECHNOLOGY UTILIZATION PUBLICATIONS: Information on technology used by NASA that may be of particular interest in commercial and other non-aerospace applications. Publications include Tech Briefs, Technology Utilization Reports and Notes, and Technology Surveys.

Details on the availability of these publications may be obtained from:

SCIENTIFIC AND TECHNICAL INFORMATION DIVISION

NATIONAL AERONAUTICS AND SPACE ADMINISTRATION

Washington, D.C. 20546